A non-stoichiometric equilibrium model for the simulation of the biomass gasification process

A non-stoichiometric equilibrium model for the simulation of the biomass gasification process*

Agostino Gambarotta, Mirko Morini†, Andrea Zubani

Department of Engineering and Architecture, University of Parma, Parco Area delle Scienze 181/a, 43125 Parma, Italy

Abstract

This paper presents a non-stoichiometric equilibrium model for the simulation of the biomass gasification process in downdraft gasifiers to be used within simulation models of complex energy systems. The chemical equilibrium is determined by minimizing the Gibbs free energy. The feedstock is composed of five elements, while fifteen chemical species are considered for the syngas. The model calculates the relative quantities of gasification products and the lower heating value of the syngas. An advantage of the non-stoichiometric approach is that it can easily calculate not only the concentrations of the main gasification products, but also the concentrations of minor products, especially the pollutant chemical species containing nitrogen and sulfur.

To analyse the behaviour of the model, a sensitivity analysis of its process parameters is presented. The model is then validated by comparing its results with the results of the

---

* The short version of the paper was presented at ICAE2016 on Oct 8-11, Beijing, China. This paper is a substantial extension of the short version of the conference paper.

† Corresponding author. Tel.: +39 0521 905714.
E-mail address: mirko.morini@unipr.it.

simulation carried out with equilibrium models and with experimental data found in literature. Finally, the model is applied to the study of the gasification of forest waste.

Keywords: biomass, gasification, pollutants, energy.

1. Introduction

Biomass gasification is one of the most promising technologies for the exploitation of energy provided by products, by-products and residues from agriculture, forestry and livestock farming [1, 2]. The main advantage of gasification is that using a gaseous fuel (i.e. syngas, which is the product of biomass gasification) is potentially more efficient than direct combustion of solid biomass, since syngas can be burned at higher temperatures. Moreover, gaseous fuels can be exploited in internal combustion engines. In this way, inefficiencies due to heat exchange can be avoided.

When dealing with white box modeling, the biomass gasification process can mainly be simulated by using three different approaches: (i) Computational Fluid Dynamic models, (ii) kinetic models and (iii) equilibrium models. Many papers have been presented in literature, though they are not reviewed in this work. Readers can refer to [3, 4].

Computational Fluid Dynamic models [5] can simulate a wide range of physical phenomena, but they need a large amount of information (e.g. detailed geometry, material properties, boundary conditions) and high computational resources.

Kinetic modeling [6] can give accurate results, in particular regarding the time evolution of the process. Nevertheless, this kind of modeling is quite complex. An

advantage of these models is that they can be suitable for studies on the influence of reactor design and process parameters (reaction rate, residence time, etc.).

Equilibrium models [1,7] are simple and fast. The equilibrium condition is essentially never reached within the gasifier, although these models can describe gasification processes with good approximation. Equilibrium models can be divided into two categories, according to the method used to calculate the chemical equilibrium: (i) stoichiometric models and (ii) non-stoichiometric models. In stoichiometric models [1], the equilibrium is determined by using the equilibrium constants for each reaction involved in the process, whereas in non-stoichiometric models [7-11] it is determined by the minimization of the Gibbs free energy.

In this paper, a non-stoichiometric equilibrium model has been developed to simulate the behavior of a downdraft gasifier. This kind of gasifier usually operates close to equilibrium conditions, so an equilibrium approach is particularly suitable. The stoichiometric approach needs a detailed specification of all the chemical reactions that occur in the reactor, but when many chemical species are involved, it can be very difficult to predict which reactions will take place. For this reason, a non-stoichiometric approach has been used in the present work.

The aim of this model is to calculate not only the concentrations of the main gasification products (carbon monoxide, molecular hydrogen, methane, carbon dioxide and water), but also the concentrations of minor products, especially the pollutant chemical species containing nitrogen and sulfur (e.g. ammonia, hydrogen sulfide). The presence of these species is not relevant in the calculation of the heating value, but it is

important to highlight whether gas treatment systems are required to remove them from the syngas or from the flue gas after syngas combustion. It should be borne in mind that the model has been developed as a mathematical tool to be used within simulation models of complex energy conversion systems.

2. Syngas composition

When dealing with gasification modelling, the focus is usually mainly related to energy issues. For this reason, syngas is generally considered to be a mixture of carbon monoxide, carbon dioxide, hydrogen, water and methane.

Nitrogen, which is present when air is taken into consideration as the oxidizer, is assumed not to participate in reactions and therefore it simply dilutes the syngas. However, a small amount of nitrogen in the oxidizer can be involved in reactions. Furthermore, biomass could contain more nitrogen and sulfur, in addition to carbon, hydrogen and oxygen. Biomass also contains inorganic species, albeit a very small amount [12]. This implies that the syngas could have a more complex composition than that reported above.

2.1 Nitrogen-based contaminants

In biomass, nitrogen is mainly present in proteins (and amino acids) together with other forms such as DNA, RNA, alkaloids, porphyrin and chlorophyll [9]. This nitrogen (generally named fuel-N) leaves the gasifier mainly as ammonia, hydrogen cyanide, nitrogen oxide, molecular nitrogen, or as heavy aromatic compounds (i.e. tar [13]). A smaller quantity is retained in solid char (i.e. char-N) [14,15]. The concentrations of

nitrogenous compounds in the syngas vary across a wide range, depending on the feedstock and on the gasification process [14]. Pyrolysis splits the fuel-N into volatile-N and char-N, while under gasification conditions the presence of gasifying agents (e.g. air, steam or oxygen) thermally cracks or reforms volatile-N and gasifies char-N, leading to the formation of hydrogen cyanide and ammonia [13]. The yield of ammonia is generally higher than the yield of hydrogen cyanide [15], leading to a concentration of ammonia in the syngas which is at least one order of magnitude higher than that of the hydrogen cyanide [16]. Ammonia is the most abundant N-based syngas contaminant, with a concentration which ranges from 350 to 18,000 ppm depending on the amount of fuel-N [17], while hydrogen cyanide is reported to have a concentration in the syngas of up to about 50 ppm and nitric oxide up to 100 ppm [18]. Finally, it should be underlined that at a sufficient temperature and residence time, molecular nitrogen becomes the predominant equilibrium product, although this condition is rarely attained in practice [16].

2.2 Sulfur-based contaminants

Biomass is characterized by a significantly lower sulfur content than coal [16]. Non-woody biomasses are characterized by a relatively higher amount of sulfur compared to woody biomass [19]. Sulfur contaminants in the syngas mostly occur as hydrogen sulfide and carbonyl sulfide. Hydrogen sulfide is always significant, since most sulfur atoms in feedstock are released as hydrogen sulfide under gasification-reducing conditions (i.e. absence of oxygen or other oxidizing agents) [19] and the concentrations in the syngas are generally around 100 ppm for woody and herbaceous biomass [17].

The concentration of carbonyl sulfide is one order of magnitude lower than hydrogen sulfide concentrations, while sulfur dioxide is present in traces [19].

3. Model development

To simplify the problem, only chemical species containing C, H, O, N and S are considered in this model. A total of 16 products are considered and assumed to be in the gaseous phase, except for unconverted solid carbon $\mathrm{C(s)}$. The global reaction inside the gasifier can be described as follows:

$$\begin{aligned}\mathrm{CH_aO_bN_cS_d} + w\ \mathrm{H_2O_{(l)}} + s\ \mathrm{H_2O_{(g)}} + e\ \mathrm{O_2} + \rho e\ \mathrm{N_2} \\ \leftrightarrow (1-\alpha)\mathrm{C_{(s)}} + n_{\mathrm{CO}}\mathrm{CO} + n_{\mathrm{CO_2}}\mathrm{CO_2} + n_{\mathrm{O_2}}\mathrm{O_2} + n_{\mathrm{CH_4}}\mathrm{CH_4} + n_{\mathrm{H_2}}\mathrm{H_2} \\ + n_{\mathrm{H_2O}}\mathrm{H_2O} + n_{\mathrm{N_2}}\mathrm{N_2} + n_{\mathrm{NO}}\mathrm{NO} + n_{\mathrm{NO_2}}\mathrm{NO_2} + n_{\mathrm{NH_3}}\mathrm{NH_3} + n_{\mathrm{HCN}}\ \mathrm{HCN} \\ + n_{\mathrm{H_2S}}\ \mathrm{H_2S} + n_{\mathrm{SO_2}}\mathrm{SO_2} + n_{\mathrm{SO_3}}\mathrm{SO_3} + n_{\mathrm{COS}}\mathrm{COS}\end{aligned} \quad (1)$$

where n_{i} is the number of moles of the i-th chemical species, ρ is the nitrogen to oxygen molar ratio in the oxidant (e.g. 3.76 for standard air) and α is a factor which accounts for the carbon not participating in the process. This factor was firstly introduced by Li et al. [10] for a fluidized bed gasifier and then updated by Damiani and Trucco in [20] for downdraft gasifiers. It is a function of the air-to-fuel ratio and it can be calculated using empirical correlations based on the interpolation of experimental results [10,20-22].

The production of tar is neglected, as is usually the case in literature when dealing with equilibrium models of downdraft reactors [1,7,20]. In fact, in this type of reactors the amount of tar leaving the gasifier is minimal. Tar production takes place in the

pyrolysis zone [23] which is upstream the hearth zone in downdraft gasifiers. This implies that the high-mass molecules [23] which constitute the tar are mainly cracked in the hearth zone.

All gaseous chemical species are considered ideal gases. All reactants are presumed to enter the reactor at temperature T_{in}, and all products are presumed to leave the reactor at the process temperature T. The process temperature is assumed to be homogeneous inside the gasifier, which is a common assumption in equilibrium models [1,7,20].

At equilibrium, the total Gibbs free energy of a gas mixture composed by M chemical species can be represented by:

$$G = \sum_{\mathrm{i}=1}^{M} n_{\mathrm{i}} G_{\mathrm{i}}^{\circ} + \sum_{\mathrm{i}=1}^{M} n_{\mathrm{i}} RT \cdot ln(n_{\mathrm{i}}/n_{\mathrm{tot}}) \quad (2)$$

where G_{i}° is the standard Gibbs free energy of the i-th species, R is the universal gas constant, T is the temperature and $n_{\mathrm{tot}} = \sum_{\mathrm{i}=1}^{M} n_{\mathrm{i}}$.

The reaction temperature is the temperature which fulfills the energy balance equation

$$\sum_{\mathrm{j}=1}^{N} n_{\mathrm{j}} \left(H_{\mathrm{f,j}}^{\circ} + \int_{T_{\mathrm{rif}}}^{T_{\mathrm{in}}} c_{\mathrm{p,j}}\, dT \right) = \sum_{\mathrm{i}=1}^{M} n_{\mathrm{i}} \left(H_{\mathrm{f,i}}^{\circ} + \int_{T_{\mathrm{rif}}}^{T} c_{\mathrm{p,i}}\, dT \right) + Q_{\mathrm{loss}} \quad (3)$$

where N is the number of reactants, H_{f}° and c_{p} are, respectively, the standard enthalpy of formation and the specific heat at constant pressure of the i-th or j-th chemical species, n is the number of moles of the i-th or j-th chemical species, and Q_{loss} is the heat lost through the reactor wall, referring to a single mole of biomass.

4. Model implementation

To calculate the composition of syngas, it is necessary to find the values of n_{i} which minimize the objective function G. This optimization problem has two families of constraints: the mass balance of the *E* elements and the non-negativity of the numbers of moles n_{i} of the chemical species in the syngas. Five mass balances, one for each element present in Eq. 1, are therefore, considered:

Balance of carbon: $n_{\mathrm{CO}} + n_{\mathrm{CO_2}} + n_{\mathrm{CH_4}} + n_{\mathrm{HCN}} + n_{\mathrm{COS}} = \alpha$

Balance of hydrogen: $4n_{\mathrm{CH_4}} + 2n_{\mathrm{H_2}} + 2n_{\mathrm{H_2O}} + 3n_{\mathrm{NH_3}} + n_{\mathrm{HCN}} + 2n_{\mathrm{H_2S}} = a + 2w + 2s$

Balance of oxygen: $n_{\mathrm{CO}} + 2n_{\mathrm{CO_2}} + 2n_{\mathrm{O_2}} + n_{\mathrm{H_2O}} + n_{\mathrm{NO}} + 2n_{\mathrm{NO_2}} + 2n_{\mathrm{SO_2}} + 3n_{\mathrm{SO_3}} + n_{\mathrm{COS}} = b + w + s + 2e$ (4)

Balance of nitrogen: $2n_{\mathrm{N_2}} + n_{\mathrm{NO}} + n_{\mathrm{NO_2}} + n_{\mathrm{NH_3}} + n_{\mathrm{HCN}} = c + 2\rho e$

Balance of sulfur: $n_{\mathrm{H_2S}} + n_{\mathrm{SO_2}} + n_{\mathrm{SO_3}} + n_{\mathrm{COS}} = d$

To solve this optimization problem, the method of Lagrange multipliers is used. For every mass balance constraint, a Lagrange multiplier λ_k is introduced. In this model, five elements are considered, so five Lagrange multipliers are introduced ($\lambda_{\mathrm{C}}, \lambda_{\mathrm{H}}, \lambda_{\mathrm{O}}, \lambda_{\mathrm{N}}, \lambda_{\mathrm{S}}$). The Lagrangian function *L* can be written as:

$$L = G - \sum_{k=1}^{E} \lambda_{\mathrm{k}} \left(\sum_{i=1}^{M} m_{\mathrm{i,k}} n_{\mathrm{i}} - W_{\mathrm{k}} \right) \quad (5)$$

where $m_{\mathrm{i,k}}$ is the number of atoms of the k-th element in the molecule of the i-th chemical species in the products, and W_{k} is the number of atoms of the k-th element in the reactants. This function is minimized when all its partial derivatives are equal to zero. This condition can be written as a system of 20 equations, 15 of which are non-linear:

$$\left(\frac{\partial L}{\partial n_{\mathrm{CO}}}\right) = \Delta G^{\circ}_{\mathrm{f,CO}} + RT\, ln\left(\frac{n_{\mathrm{CO}}}{n_{\mathrm{tot}}}\right) - \lambda_{\mathrm{C}} - \lambda_{\mathrm{O}} = 0$$
$$\left(\frac{\partial L}{\partial n_{\mathrm{CO_2}}}\right) = \Delta G^{\circ}_{\mathrm{f,CO_2}} + RT\, ln\left(\frac{n_{\mathrm{CO_2}}}{n_{\mathrm{tot}}}\right) - \lambda_{\mathrm{C}} - 2\lambda_{\mathrm{O}} = 0$$
$$\left(\frac{\partial L}{\partial n_{\mathrm{O_2}}}\right) = \Delta G^{\circ}_{\mathrm{f,O_2}} + RT\, ln\left(\frac{n_{\mathrm{O_2}}}{n_{\mathrm{tot}}}\right) - 2\lambda_{\mathrm{O}} = 0$$
$$\left(\frac{\partial L}{\partial n_{\mathrm{CH_4}}}\right) = \Delta G^{\circ}_{\mathrm{f,CH_4}} + RT\, ln\left(\frac{n_{\mathrm{CH_4}}}{n_{\mathrm{tot}}}\right) - \lambda_{\mathrm{C}} - 4\lambda_{\mathrm{H}} = 0$$
$$\left(\frac{\partial L}{\partial n_{\mathrm{H_2}}}\right) = \Delta G^{\circ}_{\mathrm{f,H_2}} + RT\, ln\left(\frac{n_{\mathrm{H_2}}}{n_{tot}}\right) - 2\lambda_{\mathrm{H}} = 0$$
$$\left(\frac{\partial L}{\partial n_{\mathrm{H_2O}}}\right) = \Delta G^{\circ}_{\mathrm{f,H_2O}} + RT\, ln\left(\frac{n_{\mathrm{H_2O}}}{n_{\mathrm{tot}}}\right) - 2\lambda_{\mathrm{H}} - \lambda_{\mathrm{O}} = 0$$
$$\left(\frac{\partial L}{\partial n_{\mathrm{N_2}}}\right) = \Delta G^{\circ}_{\mathrm{f,N_2}} + RT\, ln\left(\frac{n_{\mathrm{N_2}}}{n_{\mathrm{tot}}}\right) - 2\lambda_{\mathrm{N}} = 0$$
$$\left(\frac{\partial L}{\partial n_{\mathrm{NO}}}\right) = \Delta G^{\circ}_{\mathrm{f,NO}} + RT\, ln\left(\frac{n_{\mathrm{NO}}}{n_{\mathrm{tot}}}\right) - \lambda_{\mathrm{O}} - \lambda_{\mathrm{N}} = 0$$
$$\left(\frac{\partial L}{\partial n_{\mathrm{NO_2}}}\right) = \Delta G^{\circ}_{\mathrm{f,NO_2}} + RT\, ln\left(\frac{n_{\mathrm{NO_2}}}{n_{\mathrm{tot}}}\right) - 2\lambda_{\mathrm{O}} - \lambda_{\mathrm{N}} = 0$$
$$\left(\frac{\partial L}{\partial n_{\mathrm{NH_3}}}\right) = \Delta G^{\circ}_{\mathrm{f,NH_3}} + RT\, ln\left(\frac{n_{\mathrm{NH_3}}}{n_{\mathrm{tot}}}\right) - 3\lambda_{\mathrm{H}} - \lambda_{\mathrm{N}} = 0$$
$$\left(\frac{\partial L}{\partial n_{\mathrm{HCN}}}\right) = \Delta G^{\circ}_{\mathrm{f,HCN}} + RT\, ln\left(\frac{n_{\mathrm{HCN}}}{n_{\mathrm{tot}}}\right) - \lambda_{\mathrm{C}} - \lambda_{\mathrm{H}} - \lambda_{\mathrm{N}} = 0 \quad (6)$$
$$\left(\frac{\partial L}{\partial n_{\mathrm{H_2S}}}\right) = \Delta G^{\circ}_{\mathrm{f,H_2S}} + RT\, ln\left(\frac{n_{\mathrm{H_2S}}}{n_{\mathrm{tot}}}\right) - 2\lambda_{\mathrm{H}} - \lambda_{\mathrm{S}} = 0$$
$$\left(\frac{\partial L}{\partial n_{\mathrm{SO_2}}}\right) = \Delta G^{\circ}_{\mathrm{f,SO_2}} + RT\, ln\left(\frac{n_{\mathrm{SO_2}}}{n_{\mathrm{tot}}}\right) - 2\lambda_{\mathrm{O}} - \lambda_{\mathrm{S}} = 0$$
$$\left(\frac{\partial L}{\partial n_{\mathrm{SO_3}}}\right) = \Delta G^{\circ}_{\mathrm{f,SO_3}} + RT\, ln\left(\frac{n_{\mathrm{SO_3}}}{n_{\mathrm{tot}}}\right) - 3\lambda_{\mathrm{O}} - \lambda_{\mathrm{S}} = 0$$
$$\left(\frac{\partial L}{\partial n_{\mathrm{COS}}}\right) = \Delta G^{\circ}_{\mathrm{f,COS}} + RT\, ln\left(\frac{n_{\mathrm{COS}}}{n_{\mathrm{tot}}}\right) - \lambda_{\mathrm{C}} - \lambda_{\mathrm{O}} - \lambda_{\mathrm{S}} = 0$$

$$\left(\frac{\partial L}{\partial \lambda_{\mathrm{C}}}\right) = \alpha - n_{\mathrm{CO}} - n_{\mathrm{CO_2}} - n_{\mathrm{CH_4}} - n_{\mathrm{HCN}} - n_{\mathrm{COS}} = 0$$
$$\left(\frac{\partial L}{\partial \lambda_{\mathrm{H}}}\right) = a + 2w + 2s - 4n_{\mathrm{CH_4}} - 2n_{\mathrm{H_2}} - 2n_{\mathrm{H_2O}} - 3n_{\mathrm{NH_3}} - n_{\mathrm{HCN}} - 2n_{\mathrm{H_2S}} = 0$$
$$\left(\frac{\partial L}{\partial \lambda_{\mathrm{O}}}\right) = b + w + s + 2e - n_{\mathrm{CO}} - 2n_{\mathrm{CO_2}} - 2n_{\mathrm{O_2}} - n_{\mathrm{H_2O}} - n_{\mathrm{NO}} - 2n_{\mathrm{NO_2}} - 2n_{\mathrm{SO_2}} - 3n_{\mathrm{SO_3}} - n_{\mathrm{COS}} = 0$$
$$\left(\frac{\partial L}{\partial \lambda_{\mathrm{N}}}\right) = c - 2\rho e - 2n_{\mathrm{N_2}} - n_{\mathrm{NO}} - n_{\mathrm{NO_2}} - n_{\mathrm{NH_3}} - n_{\mathrm{HCN}} = 0$$
$$\left(\frac{\partial L}{\partial \lambda_{\mathrm{S}}}\right) = d - n_{\mathrm{H_2S}} - n_{\mathrm{SO_2}} - n_{\mathrm{SO_3}} - n_{\mathrm{COS}} = 0$$

In order to solve this minimization problem, an algorithm needs to be defined. A diagram of the solution procedure is shown in Fig. 1. The calculation of the number of

moles n_i of each product has to be nested into a cycle that calculates the process temperature (the flowchart is reported in Fig. 2).

4.1 The RAND algorithm

The calculation of the numbers of moles is performed by solving the non-linear system shown in the previous paragraph (Eq. 6). This system is solved by using the RAND algorithm [24], which is an iterative Newton-Raphson method based on the linearization of the logarithmic term in Eq. 6. The derivatives of the Lagrangian function L with respect to n_i are rearranged in the following way:

$$-\frac{1}{RT}\sum_{i=1}^{M}\left(\frac{\partial \mu_i}{\partial n_i}\right)_{n^{(q)}} \delta n_i^{(q)} + \sum_{k=1}^{E} m_{i,k}\,\delta\psi_k^{(q)} = \frac{\mu_i^{(q)}}{RT} - \sum_{k=1}^{E} m_{i,k}\,\psi_k^{(q)} \tag{7}$$

where q is the counter for the iteration, $\mu_i = n_i \Delta G^{\circ}_{f,i} + n_i RT\, ln\left(\frac{n_i}{n_{tot}}\right)$, $\psi_k = \frac{\lambda_k}{RT}$, i is the index for the chemical species in the product mixture, k is the index for the chemical element. Similarly, the derivatives of the Lagrangian function L with respect to λ_i are rearranged in the following way:

$$\sum_{i=1}^{M} m_{i,k}\,\delta n_i^{(q)} = W_k - \sum_{i=1}^{M} m_{i,k}\,n_i^{(q)}$$

The resulting linearized system can be written as:

$$Ax = B \tag{8}$$

where A is the coefficient matrix, x is the column matrix of the unknowns and B is the vector of the known terms. Vector B is shown in Appendix A while x and A are defined as follows:

$$x = [\delta n_{CO}, \delta n_{CO_2}, \delta n_{O_2}, \delta n_{CH_4}, \delta n_{H_2}, \delta n_{H_2O}, \delta n_{N_2}, \delta n_{NO}, \delta n_{NO_2}, \delta n_{NH_3}, \delta n_{HCN}, \delta n_{H_2S}, \delta n_{SO_2}, \delta n_{SO_3}, \delta n_{COS}, \delta\psi_C, \delta\psi_H, \delta\psi_O, \delta\psi_N, \delta\psi_S]^T \tag{9}$$

$$A = \begin{bmatrix} [\Gamma] & -[\Sigma]^{\mathrm{T}} \\ [\Sigma] & [\emptyset] \end{bmatrix} \quad (10)$$

where Γ is a 15x15 diagonal matrix which contains the reciprocal of the inverse of the molar concentration of the species in the syngas, Σ is a 5x15 matrix which contains the value of $m_{\mathrm{i,k}}$ and ø is a 5x5 matrix of zeros. Matrices Γ and Σ are shown in Appendix A.

After linearization, the system is solved in each iteration with respect to the new unknowns $\delta {n_{\mathrm{i}}}^{(\mathrm{q})}$ and $\delta \psi_{\mathrm{k}}^{(\mathrm{q})}$. The iterations are stopped when the absolute values of all the ratios $\frac{\delta n_{\mathrm{i}}}{n_{\mathrm{i}}}$ and $\frac{\delta \psi_{\mathrm{k}}}{n_{\mathrm{k}}}$ are lower than a small value ε. In the present work, the value $\varepsilon = 0.001$ is used.

At the end of the iteration, the values of ${n_{\mathrm{i}}}^{(\mathrm{q})}$ and ${\psi_{\mathrm{k}}}^{(\mathrm{q})}$ are updated as follows:

$${n_{\mathrm{i}}}^{(\mathrm{q}+1)} = {n_{\mathrm{i}}}^{(\mathrm{q})} - \omega^{(\mathrm{q})} \cdot \delta {n_{\mathrm{i}}}^{(\mathrm{q})} \quad (11)$$

$${\psi_{\mathrm{k}}}^{(\mathrm{q}+1)} = {\psi_{\mathrm{k}}}^{(\mathrm{q})} - \omega^{(\mathrm{q})} \cdot \delta {\psi_{\mathrm{k}}}^{(\mathrm{q})} \quad (12)$$

where $\omega^{(\mathrm{q})}$ is a coefficient calculated at each iteration according to [7] in order to force the convergence. Another purpose of ω is to keep n_{i} positive, i.e. to fulfil the constraint that imposes the non-negativity of the number of moles.

4.2 Process temperature calculation

The algorithm shown above requires knowledge of the process temperature. At the first iteration, a guess value is assumed and used to calculate the composition of syngas. These values are then used to calculate the unbalance ΔH of the energy balance equation (Eq. 3).

$$\Delta H = \sum_{\mathrm{j}=1}^{N} n_{\mathrm{j}} \left(H_{\mathrm{f,j}}^{\circ} + \int_{T_{\mathrm{ref}}}^{T_{\mathrm{in}}} c_{\mathrm{p,j}}\, dT \right) - \sum_{\mathrm{i}=1}^{M} n_{\mathrm{i}} \left(H_{\mathrm{f,i}}^{\circ} + \int_{T_{\mathrm{ref}}}^{T} c_{\mathrm{p,i}}\, dT \right) - Q_{\mathrm{loss}} \quad (13)$$

The model iteratively adjusts the temperature until ΔH approaches zero following the bisection method.

4.3 Implementation

This model has been implemented in Scilab [25]. Scilab is a free open source software for numerical computation which provides a computing environment for engineering and scientific applications. This allows the distribution and utilization of the model without a license.

The model has been also implemented in Matlab® [26], i.e. one of the most widely-used proprietary calculation software systems. The Matlab® version is similar to that of Scilab, with the exception of the RAND algorithm, which has been replaced by the *fmincon* function of the Matlab® built-in optimizer. This function, which does not have an equivalent in Scilab, has been designed for solving nonlinear programming problems. The objective function and the constraints are the same as those of the Scilab model.

The results of the two implementations were the same, confirming the reliability of the proposed algorithm. The Matlab® implemented model proved to be faster than the Scilab one, although the computing time of the Scilab model is acceptable in any case (the solution is usually found in less than 30 s using a standard laptop, e.g. i7 processor with 2.7 GHz clock and 8 GByte RAM).

5. Model analysis

A sensitivity analysis has been performed by varying the air-to-fuel ratio and biomass

moisture. In particular, the syngas composition and its lower heating value are evaluated. For the sake of readability, only the main species are reported. Figure 3 shows the results of the sensitivity analysis for the air-to-fuel ratio. In the lower abscissa, the process temperature resulting from the simulation is reported. It increases by increasing the air-to-fuel ratio (which is reported in the upper abscissa). It can be noticed that the lowest heating value decreases by increasing the process temperature. This is due to the fact that in order to reach high temperatures, the combustion process needs to proceed further. When the temperature increases, the volume fractions of carbon monoxide and molecular nitrogen increase, whereas the fractions of carbon dioxide, methane and molecular hydrogen decrease. The volume fraction of water decreases to about 1,000 K, then it increases. This increase could be due to the fact that the higher the air-to-fuel ratio, the higher the mass flow rate of the humidity which enters the gasifier with the air. Therefore, it is possible to have a reduction of the volume fraction of the water in the syngas followed by an increase.

Figure 4 shows the results of the sensitivity analysis for biomass moisture. An increase in biomass moisture causes a decrease in the lower heating value, due to the fact that a greater amount of energy is exploited for water evaporation and is therefore not available in the syngas.

6. Model validation

The model is validated by comparing the results with experimental data found in literature [20,27] and with a stoichiometric model [1]. The results are presented for

chemical species that affect the energy content of the syngas and molecular nitrogen, since in the literature only these data were available.

In Tab. 1 the results of the comparison between the present model, the experimental data from [27] and the stoichiometric model in [1] are summarized. The comparison refers to the gasification of wood (a=1.44, b=0.66, 20 % moisture on a dry basis) at a temperature of 1,073 K. It can be noticed that the model overestimates the volume fraction of molecular hydrogen and underestimates carbon monoxide and methane fractions. These lead to an error equal to 18.5 % in the evaluation of the lower heating value with respect to the experimental data, but these are well-known weaknesses of equilibrium models. In fact, comparison with the stoichiometric model [1] shows similar results.

The model is also compared to other experimental data found in Damiani and Trucco [20] by varying the air to fuel ratio. In this case, the used biomass is characterized by a=1.503 and b=0.681, and has 7.5 % moisture on dry mass. Fig. 5 shows the difference between the experimental values and the values calculated by the model, according to the following equation:

$$S = (f_s - f_m) \cdot 100 \tag{14}$$

where f_s is the experimental volume fraction of a product, and f_m is the value as calculated by the model.

It can be noticed that molecular hydrogen, carbon monoxide and water are always overestimated, while molecular nitrogen, methane and carbon dioxide are always underestimated. Moreover, the errors associated with molecular hydrogen and

molecular nitrogen have a monotonic trend. This comparison further confirms the aforementioned weaknesses of equilibrium models, a drawback that can be accepted when short simulation times are requested (e.g. when the gasification model is a component of a model of the whole energy system).

Finally, the model is compared to other non-stoichiometric models. Biagini et al in [11] developed two bi-equilibrium models and a single equilibrium model and compared them with experimental data. For the sake of brevity Fig. 6 reports the results for the case of corn cob gasification. The current model shows good agreement with the non-stoichiometric single equilibrium model presented in [11].

7. Model application

The model has been subsequently applied to forest waste gasification [26]. This biomass is assumed to have a composition characterized by a=1.4, b=0.85, c=0.02, and d=0.00004. Phyllis' [28] database reported a moisture content "as received" equal to 56.8 %, while a value of 40 % is considered in the simulation. This value is assumed to be the moisture content of the seasoned wood.

Figure 7 shows the main products of gasification and the lower heating value of syngas for different values of the air-to-fuel ratio. An increase in the air-to-fuel ratio causes an increase in oxidized compounds, and a decrease in the lower heating value. Figure 8 shows the minor products of gasification. Ammonia and hydrogen sulfide concentrations are not negligible, especially for low air-to-fuel ratio values. As reported in literature, ammonia concentration is at its highest within the nitrogen-based

contaminants, and decreases by increasing the gasification temperature [9,14,18]. Hydrogen cyanide and carbonyl sulfide are also present, but in lower concentrations. Their value increases as the air-to-fuel ratio increases.

8. Conclusions

In this paper, a non-stoichiometric equilibrium model for the simulation of biomass gasification has been developed and validated. The model takes into consideration five elements (carbon, hydrogen, oxygen, nitrogen and sulfur) in the feedstock and 15 species in the syngas. The equilibrium is calculated by minimizing the syngas Gibbs free energy.

The model is validated with respect to experimental data from literature and to the results of other equilibrium models. The model highlights the well-known weakness of equilibrium models (i.e. overestimation of molecular hydrogen and underestimation of methane). However, it should be noted that the presented model has been developed in order to define a mathematical tool to be used within simulation models of complex energy conversion systems (i.e. energy grids where the gasification process is combined with other energy conversion plants). From this point of view, the model proved to be effective in the simulation of the biomass gasification process (both for the calculation of energy-related species and pollutants), leading to errors that can be considered acceptable with reference to the calculation efforts (in terms of both calibration and execution time) and with the considered applications.

References

[1] Azzone E, Morini M, Pinelli M. Development of an equilibrium model for the simulation of thermochemical gasification and application to agricultural residues. *Renewable Energy* 2012;**46**:248-54.

[2] Field JL, Tanger P, Shackley SJ, Haefele SM. Agricultural residue gasification for low-cost, low-carbon decentralized power: An empirical case study in Cambodia. *Applied Energy* 2016; **177**:612-624.

[3] Baruah D, Baruah DC. Modeling of biomass gasification: A review. *Renewable and Sustainable Energy Reviews* 2014; **39**:806-815.

[4] Patra TK, Sheth PN. Biomass gasification models for downdraft gasifier: A state-of-the-art review. *Renewable and Sustainable Energy Reviews* 2015; **50**:583-593.

[5] Liu H, Cattolica RJ, Seiser R. CFD studies on biomass gasification in a pilot-scale dual fluidized-bed system. *International Journal of Hydrogen Energy* 2016; doi:10.1016/j.ijhydene.2016.04.205.

[6] Farid MM, Jeong HJ, Hwang J. Kinetic study on coal–biomass mixed char co-gasification with H_2O in the presence of H_2. *Fuel* 2016;**181**:1066–73.

[7] Li X, Grace JR, Watkinson AP, Lim CJ, Ergüdenler A. Equilibrium modeling of gasification: a free energy minimization approach and its application to a circulating fuidized bed coal gasifier. *Fuel* 2001;**80**:195–207.

[8] Biagini E. Study of the equilibrium of air-blown gasification of biomass to coal evolution fuels. *Energy Conversion and Management* 2016; **128**:120-133.

[9] Kilpinen P, Hupa M, Leppalahti J. Nitrogen chemistry at gasification - A thermodynamic analysis. *Abo Akademi, Turku, Finland, Report 91-14,* 1991.

[10] Li XT, Grace JR, Lim CJ, Watkinson AP, Chen HP, Kim JR. Biomass gasification in a circulating fluidized bed. *Biomass and Bioenergy* 2004; **26**:171-193.

[11] Biagini E, Barontini F, Tognotti L. Development of a bi-equilibrium model for biomass gasification in a downdraft bed reactor. *Bioresource Technology* 2016; **201**:156-165.

[12] Froment K, Defoort F, Bertrand C, Seiler JM, Berjonneau J, Poirier J. Thermodynamic equilibrium calculations of the volatilization and condensation of inorganics during wood gasification. *Fuel* 2013; **107**:269-281.

[13] Broer KM, Brown RC. The role of char and tar in determining the gas-phase partitioning of nitrogen during biomass gasification. *Applied Energy* 2015; **158**:474-483.

[14] Leppälahti J, Koljonen T, Nitrogen evolution from coal, peat and wood during gasification: Literature review. *Fuel Processing Technology* 1995; **43**:1-45.

[15] Tian FJ, Yu J, Mckenzie L, Hayashi JI, Li CZ. Gasification in Steam: A Comparative Study of Coal and Biomass. *Energy & Fuels* 2007; **21**:517-521.

[16] Woolcock P, Brown RC. A review of cleaning technologies for biomass-derived syngas. *Biomass and Bioenergy* 2013; **52**:54-84.

[17] Abdoulmoumine N, Adhikari S, Kulkarni A, Chattanathan S. A review on biomass gasification syngas cleanup: *Applied Energy* 2015; **155**:294–307.

[18] Zhou J, Masutani SM, Ishimura DM, Turn SQ, Kinoshita CM. Release of Fuel-Bound Nitrogen during Biomass Gasification. *Industrial & Engineering Chemistry Research* 2000; **39**:626-634

[19] Gai C, Dong Y, Zhang T. Distribution of sulfur species in gaseous and

condensed phase during downdraft gasification of corn straw. *Energy* 2014; **64**:248-258.

[20] Damiani L, Trucco A. Biomass gasification modelling: an equilibrium model, modified to reproduce the operation of actual reactors. *Proceedings of ASME Turbo Expo* 2009; **1**:493-502.

[21] Fu Q, Huang Y, Niu M, Yang G, Shao Z. Experimental and predicted approaches for biomass gasification with enriched air–steam in a fluidised bed. *Waste Management & Research* 2014; **32**:988-996.

[22] Aydin ES, Yucel O, Sadikoglu H. Development of a semi-empirical equilibrium model for downdraft gasification systems. *Energy* 2017; **130**:86-98.

[23] Palma CF. Modelling of tar formation and evolution for biomass gasification: A review. *Applied Energy* 2013; **111**:129-141.

[24] Smith WR, Missen RW. *Chemical reactions and equilibrium analysis*. 2nd ed. New York: Wiley; 1982.

[25] http://www.scilab.org/

[26] https://www.mathworks.com/products/matlab.html

[27] Zainal ZA, Ali R, Lean CH, Seetharamu KN. Prediction of performance of a downdraft gasifier using equilibrium modeling for different biomass material. *Energy Conversion and Management* 2001;**42**:1499–515.

[28] https://www.ecn.nl/phyllis2/Browse/Standard/ECN-Phyllis##3121

Nomenclature

A coefficient matrix

a	number of hydrogen atoms [#]
B	vector
b	number of oxygen atoms [#]
c	number of nitrogen atoms [#]
c_p	specific heat at constant pressure [J/(mol*K)]
d	number of sulfur atoms [#]
E	number of elements [#]
e	oxygen stoichiometric number [#]
f_s	experimental volume fraction of a product [-]
f_m	calculated volume fraction of a product [-]
H°	standard enthalpy of formation [J/mol]
G	total Gibbs free energy [J]
G°	standard Gibbs free energy [J/mol]
L	Lagrangian function
M	number of chemical species [#]
m	number of atoms in chemical species [#]
n	number of moles [#]
Q_{loss}	heat lost through reactor wall [J/mol biomass]
R	universal gas constant [J/(mol*K)]
S	error on volume fraction [%]
s	steam stoichiometric number [#]
T	process temperature [K]

T_{in}	reagents temperature [K]
W	number of atoms in the reagents [#]
w	moisture of biomass stoichiometric number [#]
α	fraction of carbon atoms participating in equilibrium reaction [-]
Γ	matrix as defined in Eq. A3
ε	threshold
λ	Lagrange multiplier [-]
μ	function as defined in Eq. 7
ρ	nitrogen to oxygen molar ratio in oxidant [-]
Σ	matrix as defined in Eq. A2
ψ	function as defined in Eq. 7
ω	convergence forcer [-]

Subscripts and superscripts

i	index
j	index
k	index
q	iteration counter
ref	reference
tot	total

Appendix A

The vector of the known terms *B*, with reference to Eq. 8, is defined as follows:

$$B = \begin{bmatrix} \frac{\Delta G^{\circ}_{f,CO}}{RT} + ln\left(\frac{n_{CO}}{n_{tot}}\right) - \psi_C^{(q)} - \psi_O^{(q)} \\ \frac{\Delta G^{\circ}_{f,CO_2}}{RT} + ln\left(\frac{n_{CO_2}}{n_{tot}}\right) - \psi_C^{(q)} - 2\,\psi_O^{(q)} \\ \frac{\Delta G^{\circ}_{f,O_2}}{RT} + ln\left(\frac{n_{O_2}}{n_{tot}}\right) - 2\,\psi_O^{(q)} \\ \frac{\Delta G^{\circ}_{f,CH_4}}{RT} + ln\left(\frac{n_{CH_4}}{n_{tot}}\right) - \psi_C^{(q)} - 4\,\psi_H^{(q)} \\ \frac{\Delta G^{\circ}_{f,H_2}}{RT} + ln\left(\frac{n_{H_2}}{n_{tot}}\right) - 2\,\psi_C^{(q)} \\ \frac{\Delta G^{\circ}_{f,H_2O}}{RT} + ln\left(\frac{n_{H_2O}}{n_{tot}}\right) - 2\,\psi_H^{(q)} - \psi_O^{(q)} \\ \frac{\Delta G^{\circ}_{f,N_2}}{RT} + ln\left(\frac{n_{N_2}}{n_{tot}}\right) - 2\,\psi_N^{(q)} \\ \frac{\Delta G^{\circ}_{f,NO}}{RT} + ln\left(\frac{n_{NO}}{n_{tot}}\right) - \psi_O^{(q)} - \psi_N^{(q)} \\ \frac{\Delta G^{\circ}_{f,NO_2}}{RT} + ln\left(\frac{n_{NO_2}}{n_{tot}}\right) - 2\psi_O^{(q)} - \psi_N^{(q)} \\ \frac{\Delta G^{\circ}_{f,NH_3}}{RT} + ln\left(\frac{n_{NH_3}}{n_{tot}}\right) - 3\,\psi_H^{(q)} - \psi_N^{(q)} \\ \frac{\Delta G^{\circ}_{f,HCN}}{RT} + ln\left(\frac{n_{HCN}}{n_{tot}}\right) - \psi_C^{(q)} - \psi_H^{(q)} - \psi_N^{(q)} \\ \frac{\Delta G^{\circ}_{f,H_2S}}{RT} + ln\left(\frac{n_{H_2S}}{n_{tot}}\right) - 2\,\psi_H^{(q)} - \psi_S^{(q)} \\ \frac{\Delta G^{\circ}_{f,SO_2}}{RT} + ln\left(\frac{n_{SO_2}}{n_{tot}}\right) - 2\,\psi_O^{(q)} - \psi_S^{(q)} \\ \frac{\Delta G^{\circ}_{f,SO_3}}{RT} + ln\left(\frac{n_{SO_3}}{n_{tot}}\right) - 3\,\psi_O^{(q)} - \psi_S^{(q)} \\ \frac{\Delta G^{\circ}_{f,COS}}{RT} + ln\left(\frac{n_{COS}}{n_{tot}}\right) - \psi_C^{(q)} - \psi_O^{(q)} - \psi_S^{(q)} \\ \alpha - (n_{CO}^{(q)} + n_{CO_2}^{(q)} + n_{CH_4}^{(q)} + n_{HCN}^{(q)} + n_{COS}^{(q)} \\ a + 2w + 2s - (4n_{CH_4}^{(q)} + 2n_{H_2}^{(q)} + 2n_{H_2O}^{(q)} + 3n_{NH_3}^{(q)} + n_{HCN}^{(q)} + 2n_{H_2S}^{(q)}) \\ b + w + s + 2e - (n_{CO}^{(q)} + 2n_{CO_2}^{(q)} + 2n_{O_2}^{(q)} + n_{H_2O}^{(q)} + n_{NO}^{(q)} + \delta n_{NO_2}^{(q)} + \delta n_{SO_2}^{(q)} + \delta n_{SO_3}^{(q)} + \delta n_{COS}^{(q)}) \\ c + 2\rho e - (n_{N_2}^{(q)} + n_{NO}^{(q)} + n_{NO_2}^{(q)} + n_{NH_3}^{(q)} + n_{HCN}^{(q)}) \\ d - (n_{H_2S}^{(q)} + n_{SO_2}^{(q)} + n_{SO_3}^{(q)} + n_{COS}^{(q)}) \end{bmatrix} \quad \text{(A1)}$$

The two submatrices Σ and Γ of the coefficient matrix *A*, with reference to Eq. 10, are defined as follows:

$$\Sigma = \begin{bmatrix} 1 & 1 & 0 & 1 & 0 & 0 & 0 & 0 & 0 & 0 & 1 & 0 & 0 & 0 & 1 \\ 0 & 0 & 0 & 4 & 2 & 2 & 0 & 0 & 0 & 3 & 1 & 2 & 0 & 0 & 0 \\ 1 & 2 & 2 & 0 & 0 & 1 & 0 & 1 & 2 & 0 & 0 & 0 & 2 & 3 & 1 \\ 0 & 0 & 0 & 0 & 0 & 0 & 2 & 1 & 1 & 1 & 1 & 0 & 0 & 0 & 0 \\ 0 & 0 & 0 & 0 & 0 & 0 & 0 & 0 & 0 & 0 & 0 & 1 & 1 & 1 & 1 \end{bmatrix} \quad \text{(A2)}$$

$$\Gamma = \begin{bmatrix}
-\left(\frac{n_{tot}^{(q)}}{n_{CO}^{(q)}}\right) & 0 & 0 & 0 & 0 & 0 & 0 & 0 & 0 & 0 & 0 & 0 & 0 & 0 & 0 \\
0 & -\left(\frac{n_{tot}^{(q)}}{n_{CO_2}^{(q)}}\right) & 0 & 0 & 0 & 0 & 0 & 0 & 0 & 0 & 0 & 0 & 0 & 0 & 0 \\
0 & 0 & -\left(\frac{n_{tot}^{(q)}}{n_{O_2}^{(q)}}\right) & 0 & 0 & 0 & 0 & 0 & 0 & 0 & 0 & 0 & 0 & 0 & 0 \\
0 & 0 & 0 & -\left(\frac{n_{tot}^{(q)}}{n_{CH_4}^{(q)}}\right) & 0 & 0 & 0 & 0 & 0 & 0 & 0 & 0 & 0 & 0 & 0 \\
0 & 0 & 0 & 0 & -\left(\frac{n_{tot}^{(q)}}{n_{H_2}^{(q)}}\right) & 0 & 0 & 0 & 0 & 0 & 0 & 0 & 0 & 0 & 0 \\
0 & 0 & 0 & 0 & 0 & -\left(\frac{n_{tot}^{(q)}}{n_{H_2O}^{(q)}}\right) & 0 & 0 & 0 & 0 & 0 & 0 & 0 & 0 & 0 \\
0 & 0 & 0 & 0 & 0 & 0 & -\left(\frac{n_{tot}^{(q)}}{n_{N_2}^{(q)}}\right) & 0 & 0 & 0 & 0 & 0 & 0 & 0 & 0 \\
0 & 0 & 0 & 0 & 0 & 0 & 0 & -\left(\frac{n_{tot}^{(q)}}{n_{NO}^{(q)}}\right) & 0 & 0 & 0 & 0 & 0 & 0 & 0 \\
0 & 0 & 0 & 0 & 0 & 0 & 0 & 0 & -\left(\frac{n_{tot}^{(q)}}{n_{NO_2}^{(q)}}\right) & 0 & 0 & 0 & 0 & 0 & 0 \\
0 & 0 & 0 & 0 & 0 & 0 & 0 & 0 & 0 & -\left(\frac{n_{tot}^{(q)}}{n_{NH_3}^{(q)}}\right) & 0 & 0 & 0 & 0 & 0 \\
0 & 0 & 0 & 0 & 0 & 0 & 0 & 0 & 0 & 0 & -\left(\frac{n_{tot}^{(q)}}{n_{HCN}^{(q)}}\right) & 0 & 0 & 0 & 0 \\
0 & 0 & 0 & 0 & 0 & 0 & 0 & 0 & 0 & 0 & 0 & -\left(\frac{n_{tot}^{(q)}}{n_{H_2S}^{(q)}}\right) & 0 & 0 & 0 \\
0 & 0 & 0 & 0 & 0 & 0 & 0 & 0 & 0 & 0 & 0 & 0 & -\left(\frac{n_{tot}^{(q)}}{n_{SO_2}^{(q)}}\right) & 0 & 0 \\
0 & 0 & 0 & 0 & 0 & 0 & 0 & 0 & 0 & 0 & 0 & 0 & 0 & -\left(\frac{n_{tot}^{(q)}}{n_{SO_3}^{(q)}}\right) & 0 \\
0 & 0 & 0 & 0 & 0 & 0 & 0 & 0 & 0 & 0 & 0 & 0 & 0 & 0 & -\left(\frac{n_{tot}^{(q)}}{n_{COS}^{(q)}}\right)
\end{bmatrix} \quad \text{(A3)}$$

Table Captions

Table 1. Model validation (a=1.44, b=0.66, biomass moisture equal to 20 %, process temperature equal to 1073 K)

Table 1. Model validation (a=1.44, b=0.66, biomass moisture equal to 20 %, process temperature equal to 1073 K)

	volume fraction (dry basis) [%]			Absolute difference [%]		Relative difference [%]	
Chemical species	Current model	Exp. Data in [27]	Model in [1]	With respect to [27]	With respect to [1]	With respect to [27]	With respect to [1]
CO	21.57	23.04	20.80	-1.47	0.77	-6.4	3.7
H_2	25.00	15.23	23.39	9.77	1.61	64.1	6.9
CH_4	0.04	1.58	0.75	-1.54	-0.71	-97.5	-94.7
N_2	41.66	42.31	42.74	-0.65	-1.08	-1.5	-2.5
CO_2	11.73	16.42	12.31	-4.69	-0.58	-28.6	-4.7
	LHV (dry basis) [kJ/kg]			Absolute difference [kJ/kg]		Relative difference [%]	
	Current model	Exp. Data in [27]	Model in [1]	With respect to [27]	With respect to [1]	With respect to [27]	With respect to [1]
	5211	4398	5103	813	108	18.5	2.1

Figure Captions

Fig. 1. Flow chart for the calculation procedure

Fig. 2. Flow chart for the calculation of the numbers of moles.

Fig. 3. Air-to-fuel ratio sensitivity analysis (biomass: *a*=1.54, b=0.62; moisture on dry basis: 16 %; oxidant: standard air)

Fig. 4. Biomass moisture sensitivity analysis (biomass: *a*=1.54, b=0.62; oxidant: standard air; air-to-fuel ratio equal to 2.0)

Fig. 5. Model validation by varying the air to fuel ratio (biomass: *a*=1.503, b=0.681; moisture on dry basis: 7.5 %; oxidant: standard air)

Fig. 6: Model validation (biomass: a=1.54, b=0.65; moisture on dry basis: 10.1 %; oxidant: standard air; air-to-fuel ratio equal to 1.2)

Fig. 7. Model application to forest waste gasification: main products

Fig. 8. Model application to forest waste gasification: minor products

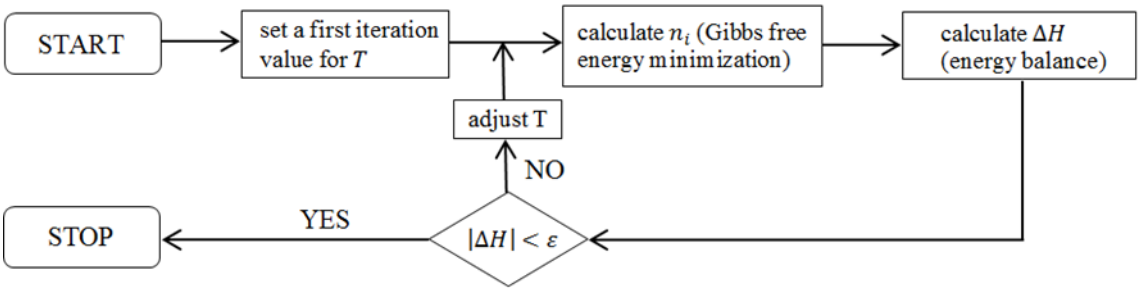

Fig. 1. Flow chart for the calculation procedure

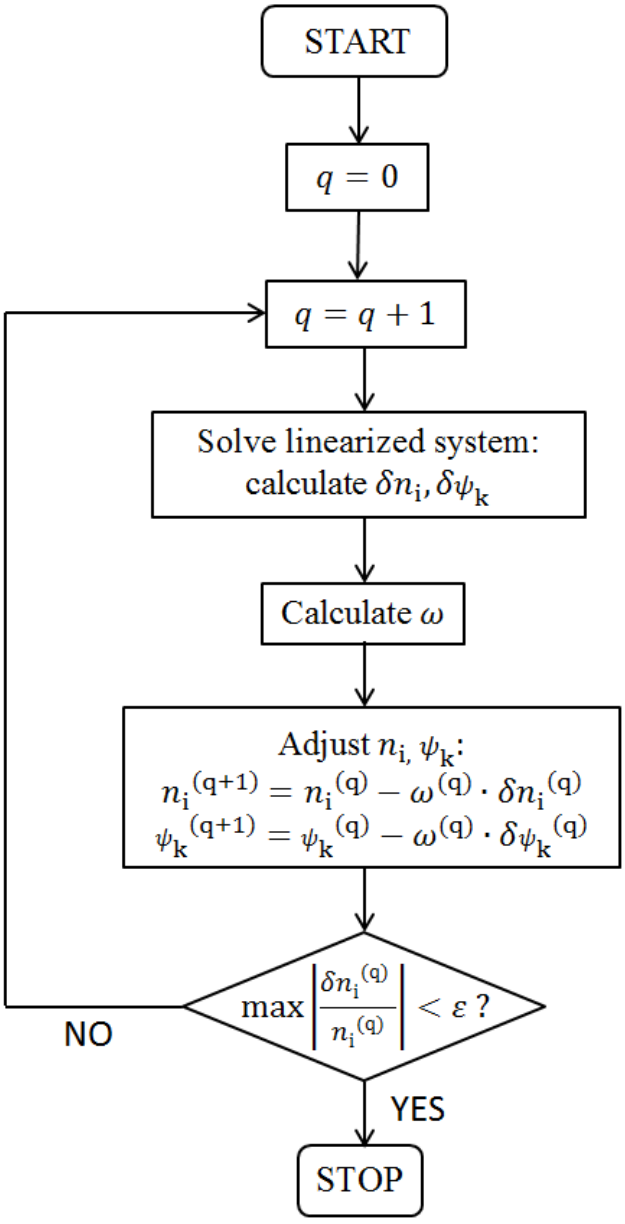

Fig. 2. Flow chart for the calculation of the numbers of moles.

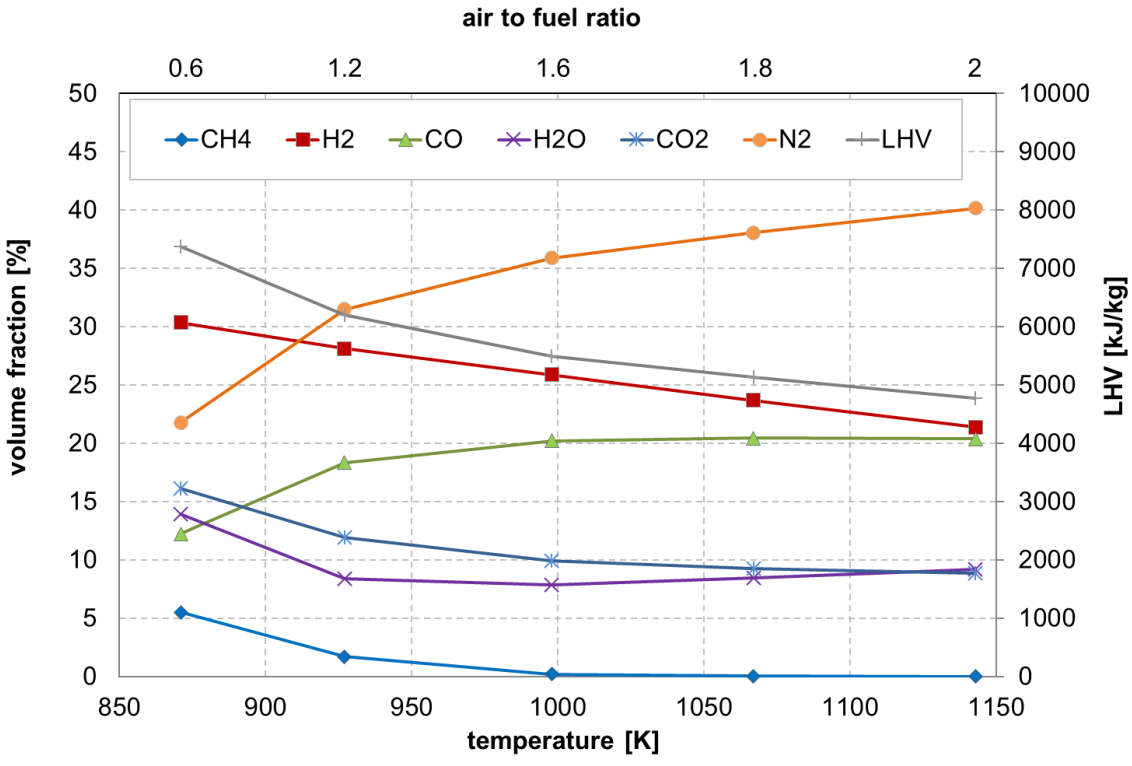

Fig. 3. Air-to-fuel ratio sensitivity analysis (biomass: *a*=1.54, b=0.62; moisture on dry basis: 16 %; oxidant: standard air)

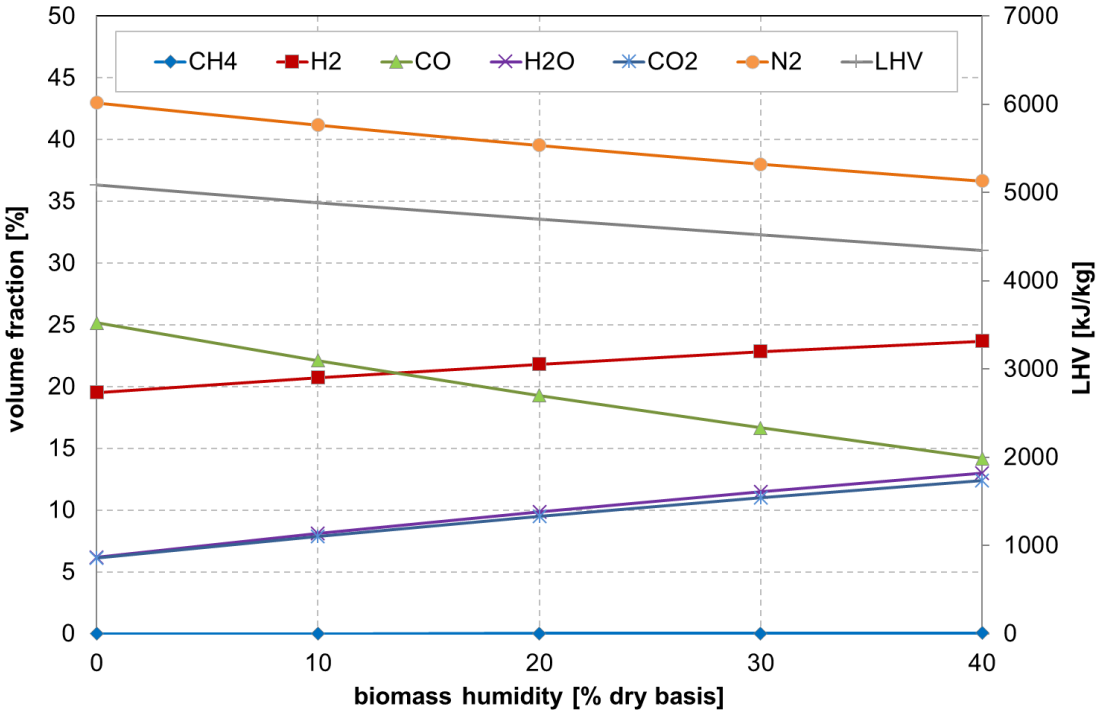

Fig. 4. Biomass moisture sensitivity analysis (biomass: *a*=1.54, b=0.62; oxidant: standard air; air-to-fuel ratio equal to 2.0)

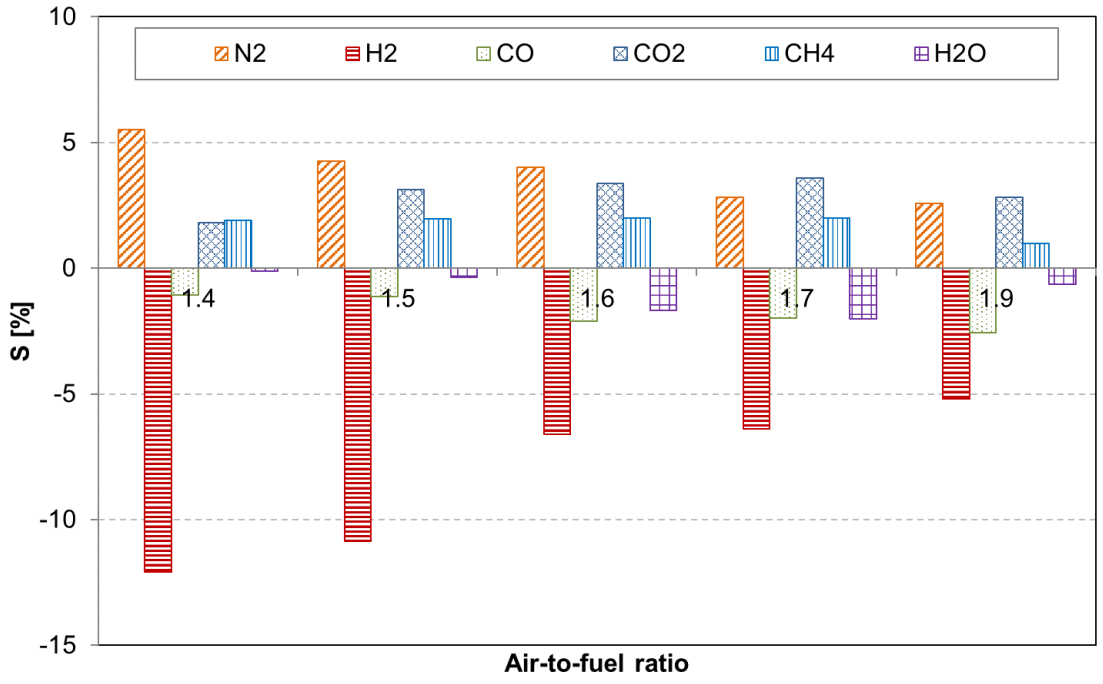

Fig. 5. Model validation by varying the air to fuel ratio (biomass: *a*=1.503, b=0.681; moisture on dry basis: 7.5 %; oxidant: standard air)

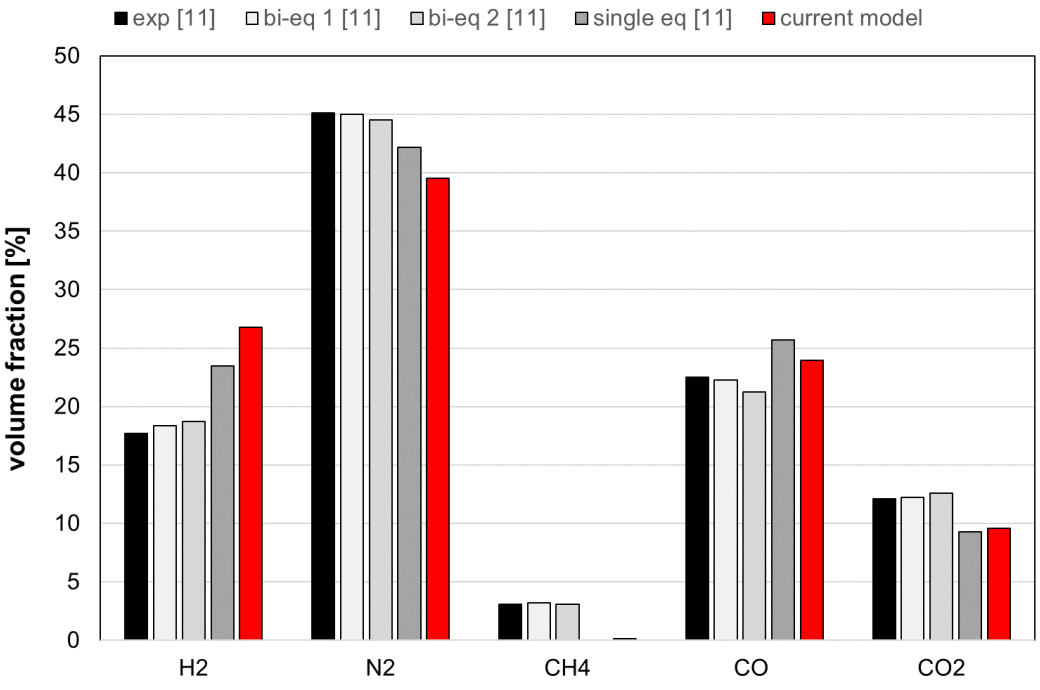

Fig. 6: Model validation (biomass: a=1.54, b=0.65; moisture on dry basis: 10.1 %; oxidant: standard air; air-to-fuel ratio equal to 1.2)

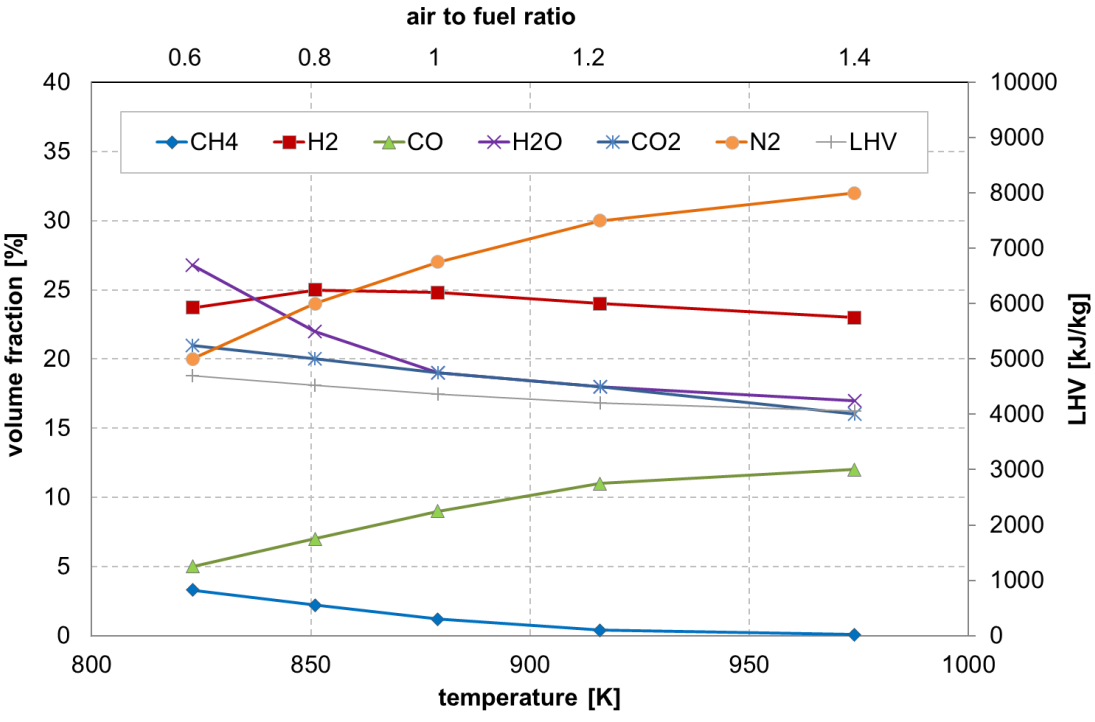

Fig. 7. Model application to forest waste gasification: main products

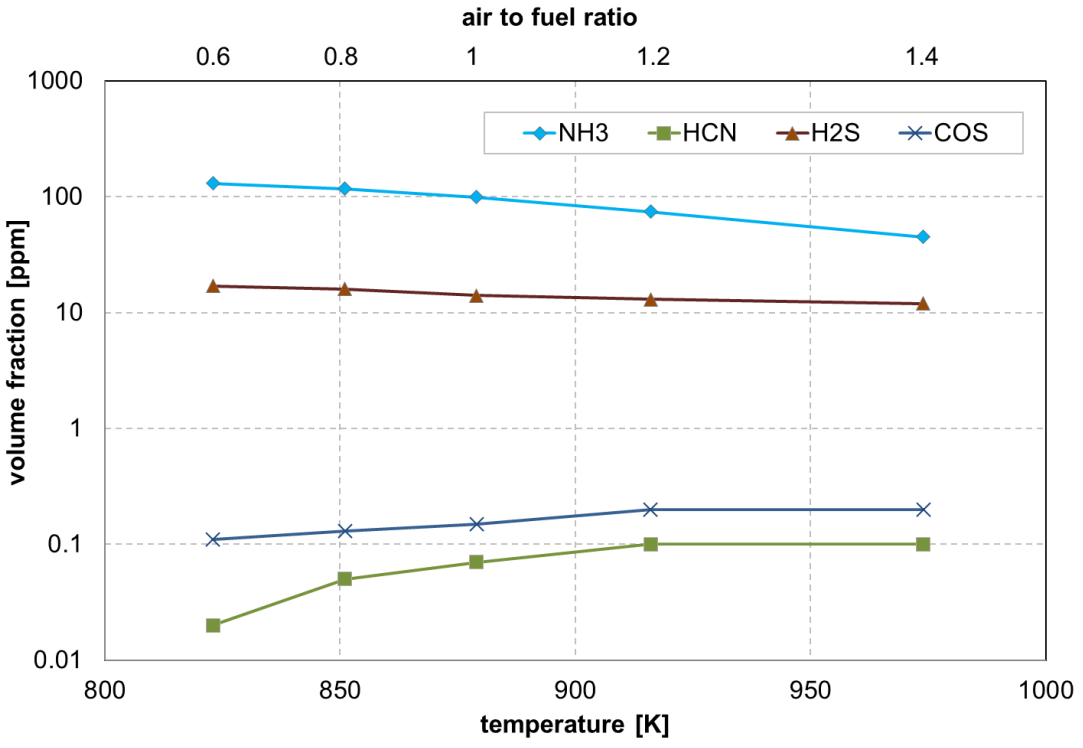

Fig. 8. Model application to forest waste gasification: minor products